ChemPubSoc Europe

DOI: 10.1002/cctc.201402808

CHEMCATCHEM Full Papers

Highly Effective Pt-Based Water–Gas Shift Catalysts by Surface Modification with Alkali Hydroxide Salts

Matthias Kusche,[a] Karen Bustillo,[b] Friederike Agel,[a] and Peter Wasserscheid*[a]

Herein, we describe an economical and convenient method to improve the performance of Pt/alumina catalysts for the water–gas shift reaction through surface modification of the catalysts with alkali hydroxides according to the solid catalyst with ionic liquid layer approach. The results are in agreement with our findings reported earlier for methanol steam reforming. This report indicates that alkali doping of the catalyst plays an important role in the observed catalyst activation. In addition, the basic and hygroscopic nature of the salt coating contributes to a significant improvement in the performance of the catalyst. During the reaction, a partly liquid film of alkali hydroxide forms on the alumina surface, which increases the availability of H_2O at the catalytically active sites. Kinetic studies reveal a negligible effect of the KOH coating on the rate dependence of CO and H_2O partial pressures. TEM studies indicate an agglomeration of the active Pt clusters during catalyst preparation; restructuring of Pt nanoparticles occurs under reaction conditions, which leads to a highly active and stable system over 240 h time on stream. Excessive pore fillings with KOH introduce a mass transfer barrier as indicated in a volcano-shaped curve of activity versus salt loading. The optimum KOH loading was found to be 7.5 wt%.

Introduction

The water–gas shift reaction (WGSR) is among the most relevant reactions for the industrial production of synthesis gas and H_2. Moreover, the WGSR is used for balancing synthesis gas during ammonia, Fischer–Tropsch, or methanol synthesis.[1] In the WGSR, CO reacts with H_2O to yield one equivalent of H_2 and one equivalent of CO_2 in a mildly exothermic transformation [Eq. (1)].

$$CO + H_2O \rightarrow CO_2 + H_2 \qquad \Delta H^\circ_{298} = -41.2\ kJ\ mol^{-1} \qquad (1)$$

The industrial WGS process is typically divided into a high-temperature and a low-temperature reaction step to obtain both high rates (triggered by the high temperature in the first reactor) and high CO conversion (enabled by the low temperature in the second reactor). The high-temperature shift reaction is usually performed over a Fe_2O_3/Cr_2O_3 catalyst at temperatures between 300 and 500 °C. Subsequently, the low-temperature shift reaction proceeds over $Cu/ZnO/Al_2O_3$ catalysts in the temperature range of 200–250 °C, which leads to a reduction in CO content to the amount remaining in exhaust gas (≈0.3%).

The WGSR has recently attracted additional attention in the context of H_2-based energy systems and onboard fuel reforming. If H_2 is used in a proton exchange membrane fuel cell, the CO concentration in the feed gas has to be reduced to 10 ppm. Otherwise, a degradation of the Pt-based fuel cell catalyst is inevitable. One option to reduce CO contamination in a H_2 feed from syngas is to apply gas purification steps such as adsorption or preferential oxidation of CO. Alternatively, the low-temperature shift step can be operated at temperatures as low as possible to further increase the thermodynamic driving force for high CO conversions.[2] Moreover, the WGSR for mobile applications requires dynamic operation in frequent on–off cycles in miniaturized equipment with high space–time yields. This necessitates the development of improved catalyst systems for the WGSR.[3]

The state-of-the-art industrial $Cu/ZnO/Al_2O_3$ catalyst system exhibits several drawbacks, such as pyrophoric nature, deactivation during standby, and the need for extensive preformation procedures, before the operation.[4] Several noble metal catalysts on oxidic supports have been reported to circumvent the named limitations of the conventional Cu-based WGSR catalysts. Two different classes of support materials have been used: a) reducible supports such as ceria and titania; b) nonreducible supports such as silica, magnesia, and alumina.[5,6,7] Pt

[a] M. Kusche, Dr. F. Agel, Prof. P. Wasserscheid
Lehrstuhl für Chemische Reaktionstechnik
Friedrich-Alexander-Universität Erlangen-Nürnberg
Egerlandstraße 3
91058 Erlangen (Germany)
Fax: (+49) 9131-8527421
E-mail: wasserscheid@crt.cbi.uni-erlangen.de
Homepage: http://www.crt.cbi.uni-erlangen.de

[b] Dr. K. Bustillo
National Center for Electron Microscopy
Molecular Foundry
Lawrence Berkeley National Lab
Berkeley, CA 94720 (USA)

Supporting information for this article is available on the WWW under http://dx.doi.org/10.1002/cctc.201402808.

has been found to be a suitable metal for the WGSR if non-phyrophoric and robust WGSR systems are needed for dynamic H_2 production scenarios.[7,8]

Herein, we present a new way to improve the performance of Pt-based WGSR catalysts through surface modification of the catalyst with molten alkali salts. The concept of this study is related to our recently published studies demonstrating catalyst optimization for methanol steam reforming.[9,10] Because the WGSR is part of the methanol steam reforming reaction network,[11] we were interested in studying the effect of surface modification of the catalyst with molten alkali salts on the WGSR alone.

The general idea of modifying the surface of a heterogeneous catalyst through a thin film of molten salt is not new. In the literature, this procedure has been extensively investigated by us and other groups with use of low-melting salts, referred to as ionic liquids; the term "SCILL" (solid catalyst with ionic liquid layer) has been coined for this approach.[12] SCILL systems make use of specific physicochemical properties of the ionic liquid, and they rely on the chemical interaction of the salt with the catalytically active sites of the applied heterogeneous catalyst. Under the conditions of the continuous gas phase reaction, the film of the ionic liquid resides on the catalyst surface owing to the extremely low vapor pressure of these liquid salts.[13]

By the application of SCILL-systems, significant effects on selectivity have been observed, for example, in hydrogenation catalysis.[14] Comprehensive surface science studies have elucidated the molecular origin of the observed alterations by demonstrating that certain surface sites of catalytic nanoparticles are poisoned in a selective manner by the molten salt coating.[15]

From our previous research, we know that ionic liquids involving organic heterocyclic cations are not stable under WGSR conditions. The imidazolium ion, for example, undergoes ring hydrolysis at temperatures above 180 °C in the presence of water vapor.[16] Consequently, in our previous studies of salt-modified catalysts for methanol steam reforming, we selected inorganic molten salts for catalyst coating. We initially used a mixture of Li/K/Cs[OAc] (molar ratio = 0.2/0.275/0.525).[17] On the basis of the initial results with mixed acetate salts, we extended our selection to alkali hydroxides and carbonates. During methanol steam reforming, it was demonstrated that regardless of the melting point of the H_2O-free salt, a highly concentrated salt solution forms in the catalyst pores under the reaction conditions.[9,10]

On the basis of these previous results, this study uses the concept of modifying Pt/alumina catalysts by a salt coating for the WGSR. The salt-modified Pt catalysts were synthesized by adding a defined amount of salt in the form of an aqueous solution to the heterogeneous catalyst. The solvent was removed during vacuum evacuation, and the sample was subjected to a final drying step ($T = 150$ °C, $p < 0.1$ mbar, 4 h; 1 mbar = 0.1 kPa). The resulting catalyst material was not calcined. The amount of applied salt(s) resulted in a certain mass load, and w was the mass of salt divided by the mass of the uncoated Pt/alumina catalyst. All WGSR experiments were performed in a continuously operated fixed-bed reactor (see the Supporting Information for details). The catalyst was brought into contact with a dilute stream of H_2O and CO in an equimolar ratio (4.0 bar N_2, 0.5 bar CO, 0.5 bar H_2O; 1 bar = 100 kPa); the residence time τ was adjusted to 0.75 s.

In the case of methanol steam reforming, we quickly found that although all alkali salt coatings showed activating effects, coating with alkali hydroxides was most effective.[9,10] Therefore, the results reported herein are restricted to alkali hydroxide coatings; especially, KOH has extensively been probed as a catalyst modifier.

Results and Discussion

The performance of the uncoated Pt/alumina catalyst for the WGSR is shown in Figure 1 ($T = 230$ °C) and compared to a variation in KOH salt coating on the same catalyst (salt loading $w_{KOH} = 3.8$, 7.5, 17.2, 30.0 wt%).

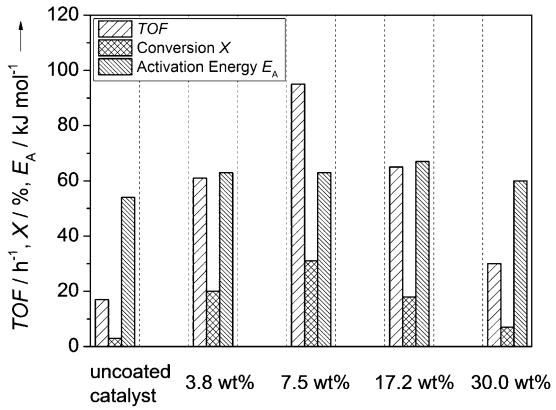

Figure 1. Comparison of Pt/alumina catalysts with varying KOH surface coatings ($w_{KOH} = 0$, 3.8, 7.5, 17.2, 30.0 wt%) during the continuous WGSR. Reaction conditions for all loadings: $T = 230$ °C, $p_{total} = 5$ bar, inert gas N_2, $p_{CO} = p_{H_2O} = 0.5$ bar, $m_{catalyst} = 401.4$ mg, $n_{Pt} = 1 \times 10^{-4}$ mol, $\tau = 0.5$–0.85 s.

A comparison of turnover frequencies (TOFs) and CO conversions demonstrates that the KOH coating of the initial Pt catalyst with an optimum salt loading of 7.5 wt% results in a sixfold increase in activity ($TOF_{w=7.5\,wt\%\,KOH} = 95\ h^{-1}$ vs. $TOF_{w=0\,wt\%\,KOH} = 17\ h^{-1}$. A lower KOH loading of 3.8 wt% does not appear to be sufficient to fully activate the surface of the Pt/alumina catalyst. Modification with a salt loading of ≥ 17.2 wt% was again found to be unfavorable and resulted in a steep decline in activity ($TOF_{w=17.2\,wt\%\,KOH} = 65\ h^{-1}$ and $TOF_{w=30.0\,wt\%\,KOH} = 30\ h^{-1}$). These results are in good agreement with our findings for the methanol steam reforming reaction.[9,10] For the latter reaction, we showed that higher KOH loadings resulted in diffusional limitations. Notably, the applied amounts of KOH result in a low pore filling degree based on the dry mass of KOH but in a much higher pore filling in the H_2O-saturated state under WGSR conditions.

The apparent Arrhenius activation energy of the WGSR (based on a temperature variation between 200 and 230 °C in steps of 10 °C) is evidently affected by surface modification

with KOH. For the uncoated reference catalyst, an apparent activation energy of 54 kJ mol^{-1} was found, whereas the KOH-modified catalysts resulted in activation energy values in the range of 63–67 kJ mol^{-1}. In addition to a change in reaction mechanism and/or an altered adsorption behavior of reactants, the salt coating may cause a variation in concentrations/activities of reactants or products with temperature at the reactive site and such effects would also be included in our reported activation energy values.

In a next set of experiments, we were interested to know whether the observed activating effects were unique to the potassium salt or whether they could also be accomplished with other alkali hydroxide coatings. Consequently, we also tested LiOH-, NaOH-, and CsOH-modified catalysts; the molar amount of alkali hydroxide was kept constant at the optimum loading found for KOH (w_{KOH} = 7.5 wt%). Thus, salt coatings of 3.2 wt% LiOH, 5.4 wt% NaOH, and 20.0 wt% CsOH were applied, respectively. In addition, we screened catalysts with one higher (w_{LiOH} = 20.0 wt% w_{NaOH} = 20.0 wt%) and one lower (w_{CsOH} = 7.5 wt%) salt loading to quickly ascertain the effect of varying salt loadings on these other alkali hydroxides. All experiments were performed in the temperature range of 200–230 °C. These results are given in the Supporting Information.

All catalysts coated with an alkali hydroxide salt demonstrated improved catalytic performance than the unmodified reference catalyst. The maximum increase in WGSR activity was achieved with KOH (w_{KOH} = 7.5 wt%) and NaOH (w_{NaOH} = 20 wt%) coatings, with TOF = 95 h^{-1} for the KOH-modified catalyst and TOF = 86 h^{-1} for the NaOH-modified catalyst. In our former work using diffuse reflectance infrared Fourier transform spectroscopy to study methanol steam reforming, we found[9,10] that during the impregnation with alkali hydroxides, the CO adsorption mechanism was shifted from the on-top position of CO at terraces and particle edges to CO in a bridged conformation at terraces.[10] These effects are described in the literature under the term "alkali doping" and have been verified through a series of surface science studies.[18,19,20] There are also literature reports on the enhanced catalytic activity of Pt-based WGSR catalysts on various supports (Al_2O_3, CeO_2, and C) after the addition of Na or K species during a conventional catalyst preparation method involving impregnation, calcination, and activation of the respective catalyst.[8, 21,22] Along these lines, Liu et al. recently reported that the addition of K_2CO_3 during the preparation of a Ru-based catalyst led to an increased reaction rate of the WGSR.[23]

In the case of hydroxide salt coatings, the salt's basicity and hygroscopicity adds to the known modification of the CO adsorption behavior. There has been a lively debate as to whether a formate/carbonate[22,24,25] or a carboxylate[5,26,27,28] compound is the key intermediate in the WGSR network. The decomposition of such intermediates, the dissociative activation of H_2O, and the surface diffusion of OH^- have all been identified as the rate-limiting steps during catalysis using Pt particles in the WGSR.[5,24,25,26,29] We assume that owing to the KOH coating on the catalyst, an extensive amount of OH^- is present on the catalyst surface. Consequently, all steps involving OH^- are strongly accelerated. In addition, the hygroscopic nature of alkali hydroxides, as verified by dynamic vapor sorption,[10] combined with the support basicity, facilitates dissociative adsorption of H_2O on the alumina support and diffusion toward the interface between catalytically active Pt nanoparticles and alumina. The electronic modification of the active Pt sites by K^+ and the alteration of the support by OH^- both contribute to the increase in WGSR activity. In a next set of experiments, we were interested to know whether the observed activation through alkali hydroxide salt coating is a permanent effect, that is, whether the effect remains constant over long catalyst operating times.

Stability experiment with the KOH-coated Pt/alumina catalyst in the WGSR

To investigate the stability of the catalyst and the KOH salt coating, the Pt/alumina catalyst impregnated with KOH (w_{KOH} = 7.5 wt%) was operated for 240 h time on stream in a continuous WGSR under alternating process conditions (Figure 2).

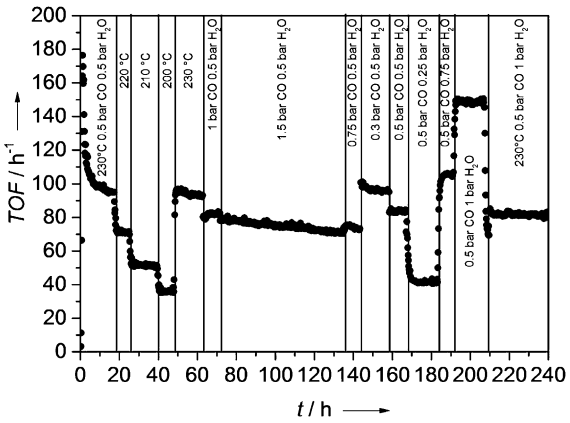

Figure 2. Results of long-term continuous WGSR experiments with the Pt/alumina catalyst coated with KOH at w_{KOH} = 7.5 wt%. Reaction conditions: T = 230–200 °C, p_{total} = 5 bar, inert gas N_2, T = 230 °C (if not indicated otherwise), $p_{CO} = p_{H_2O}$ = 0.5 bar (if not indicated otherwise), $m_{catalyst}$ = 401.4 mg, $n_{Pt} = 1 \times 10^{-4}$ mol, τ = 0.5–0.7 s, variation in p_{CO} = 0.3–1.5 bar and p_{H_2O} = 0.25–1 bar.

After a 10 h induction phase, in which catalyst deactivation is observed, the system reaches stable operating conditions (TOF = 95 h^{-1} at t = 18 h). During temperature variation (T = 200–230 °C, t = 18–63 h), an apparent activation energy of 63 kJ mol^{-1} was determined (see Figure 2). If the CO concentration is varied, the catalyst shows minor deactivation at high CO partial pressures (p_{CO} > 1 bar). Upon reaching standard conditions again (T = 230 °C, $p_{CO} = p_{H_2O}$ = 0.5 bar, t = 160 h), the catalyst shows stable performance with TOF = 84 h^{-1}. After variation in p_{H_2O} (p_{H_2O} = 0.25–1 bar, t = 169–240 h), the catalyst shows stable performance at TOF = 84 h^{-1} up to the end of the experimental run (t = 240 h). Thus, we demonstrated that the KOH salt coating leads to a stable catalyst performance over at least 10 days with no visible KOH leaching and no systematic decline in catalyst activity (apart from the region of high CO partial pressures in which coke formation is likely).[1]

Kinetic studies

In a next set of experiments, we studied the effect of surface modification with KOH on the kinetics of the WGSR catalyst under realistic process conditions, such as variation in CO and H_2O partial pressures. These experiments were performed at $T = 230\,^{\circ}C$ and $p_{total} = 5$ bar with the same mass of the catalyst in every experimental run. After reaching steady state, p_{CO} was varied from 0.3 to 1.5 bar at a constant p_{H_2O} of 0.5 bar. Subsequently, p_{H_2O} was increased from 0.25 to 1 bar at a p_{CO} of 0.5 bar. The pressure balance was closed by using N_2 as inert gas. It was ensured that the conversion of CO was always less than 25% so that the experiments in the plug flow reactor were always under differential conditions (except for steps with $p_{CO} = 0.3$ bar and $p_{H_2O} = 1$ bar for the catalyst with $w_{KOH} =$ 7.5 wt%).

All experimental data were evaluated by using a power law model. The backward reaction (reverse WGSR) was neglected owing to the low conversion and the large distance from the equilibrium under the applied reaction conditions. Under these conditions (constant volume flow), the effective reaction rate r_{eff} correlates with TOF values as shown in Equation (2).

$$r_{eff} \cong \mathrm{TOF} = k_{eff} p_{CO}^{n} p_{H_2O}^{m} \qquad (2)$$

The rate law was intentionally kept simple to study the effect of surface modification with KOH on WGSR kinetics. The dependence of TOF on p_{CO} for the uncoated Pt catalyst and the Pt catalysts coated with 7.5 and 17.2 wt% KOH is shown in Figure 3. The corresponding results of the variation in p_{H_2O} for the same catalysts are presented in Figure 4.

A reaction order for CO, n, is derived from the variation in p_{CO}, which lies in-between −0.14 and −0.18 for the three investigated catalysts. Thus, the KOH salt coating has little effect on the rate dependence of CO partial pressure. The slightly

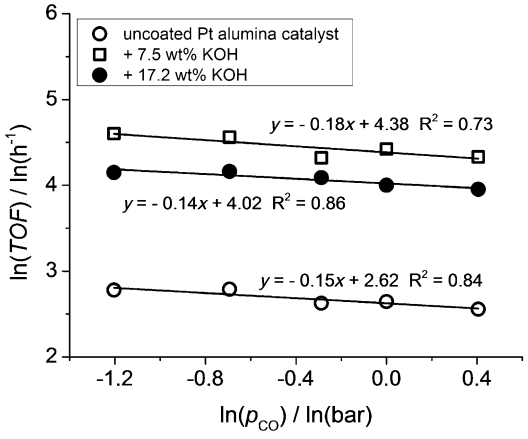

Figure 3. Variation in partial pressure of CO for Pt/alumina catalysts with different KOH loadings ($w_{KOH} = 0$ wt%, $w_{KOH} = 7.5$ wt%, and $w_{KOH} = 17.1$ wt%) in the continuous WGSR. Reaction conditions: $T = 230\,^{\circ}C$, $p_{total} = 5$ bar, inert gas N_2, $p_{H_2O} = 0.5$ bar, $m_{catalyst} = 401.4$ mg, $n_{Pt} = 1 \times 10^{-4}$ mol, $\tau = 0.5$–0.7 s, variation in $p_{CO} = 0.3$–1.5 bar.

negative reaction order for CO reflects the strong CO adsorption on the Pt active sites that impedes coordination of H_2O and thus slows down the reaction.

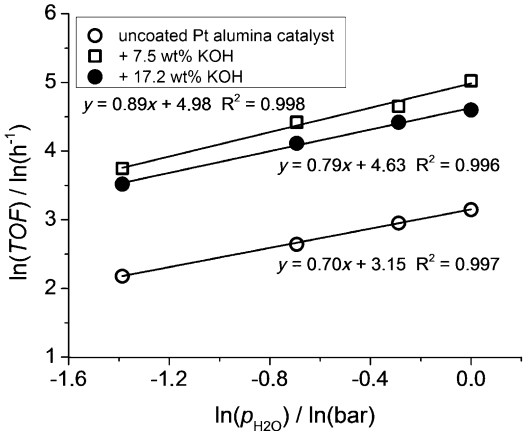

Figure 4. Variation in partial pressure of H_2O for Pt/alumina catalysts with different KOH loadings ($w_{KOH} = 0$ wt%, $w_{KOH} = 7.5$ wt%, and $w_{KOH} = 17.2$ wt%) in the continuous WGSR. Reaction conditions: $T = 230\,^{\circ}C$, $p_{total} = 5$ bar, inert gas N_2, $p_{CO} = 0.5$ bar, $m_{catalyst} = 401.4$ mg, $n_{Pt} = 1 \times 10^{-4}$ mol, $\tau = 0.5$–0.7 s, variation in $p_{H_2O} = 0.25$–1 bar.

The reaction order for H_2O, m, is determined from the variation in p_{H_2O} (Figure 4); the m values indicate a small effect on the reaction rate owing to the salt coating. Although m for the uncoated reference catalyst was found to be 0.7, both salt-impregnated catalysts showed a slightly higher dependence of the reaction rate on H_2O partial pressure ($m_{w=7.5\,wt\%\,KOH} = 0.9$ and $m_{w=17.2\,wt\%\,KOH} = 0.8$).

In conclusion, we found that reaction orders are not significantly altered by KOH coating and are still in good agreement with kinetic data for the Pt/alumina WGSR catalyst reported in the literature.[6,30] Thus, the drastic increase in WGSR activity is due to an increase in k_{eff}. From literature reports on Pt catalysts, it is known that the surface diffusion of OH^- to the active Pt sites to decompose the carbon intermediate limits the catalytic activity of the WGSR.[5,24,29,31] On the basis of this information, we assume that the KOH coating affects this diffusion step in a strongly positive manner.

TEM studies

TEM was used to ascertain the effect of the salt coating on the Pt particle size and agglomeration both before and after the WGSR. For analysis, 100–125 Pt nanoparticles were evaluated, which yielded a normal distribution of particle diameter. Conditions for the WGSR were as follows: $t = 300$ h, $T = 200$–$230\,^{\circ}C$, $p_{total} = 5$ bar, $p_{CO} = 0.3$–1.5 bar, and $p_{H_2O} = 0.25$–1 bar. Notably, water vapor present under WGSR conditions also affects the structure of the alumina support material. The uncoated Pt/alumina catalysts before and after the WGSR are shown in Figures 5 and 6, respectively, and the KOH-coated Pt/alumina catalysts before and after the WGSR are shown in Figures 7 and 8.

Before the WGSR, the Pt nanoparticles were homogeneously distributed on the surface with a mean cluster diameter of 2.66 (arithmetic mean) to 2.81 nm (center of Gaussian distribu-

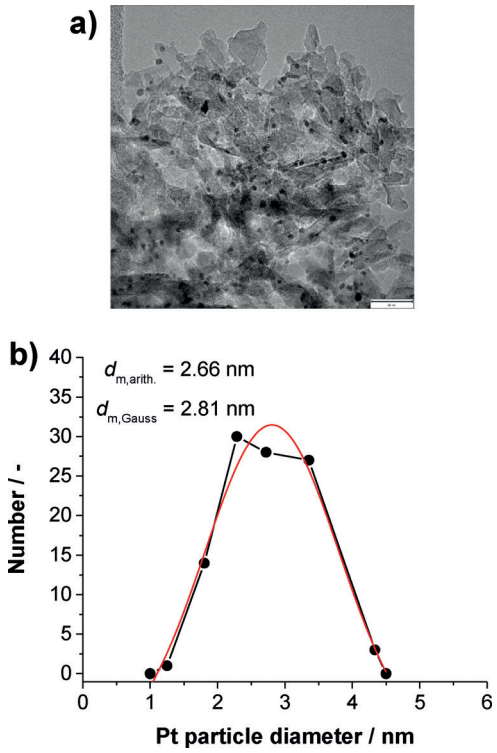

Figure 5. The uncoated Pt/alumina catalyst before the WGSR. a) Bright-field image acquired with a Philips CM300 transmission electron microscope at 300 kV; scale bar = 20 nm. For further analysis of Pt particles see the Supporting Information. b) Mean particle diameter obtained from evaluating 100 particles. Data are plotted in black, with Gaussian fit in red.

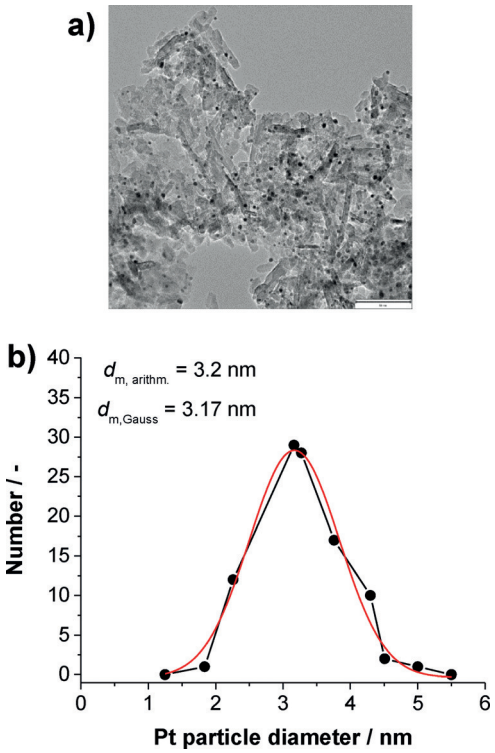

Figure 6. The uncoated Pt/alumina catalyst after the WGSR (T = 200–230 °C, p_{CO} = 0.3–1.5 bar, p_{H_2O} = 0.25–1 bar, t_R = 300 h). a) Bright-field image acquired with a Philips CM300 transmission electron microscope at 300 kV; scale bar = 50 nm. b) Mean particle diameter obtained from evaluating 100 particles. Data are plotted in black, with Gaussian fit in red.

tion). These values are in good agreement with the results of TEM and CO chemisorption analyses that we performed for the same catalyst in a former work.[10] As expected, only a small change was found after the WGSR. The TEM analysis reveals a small increase in the mean diameter of Pt nanoparticles, from 2.7 to 3.2 nm; however, the particles are still homogeneously distributed over the catalyst surface with a Gaussian distribution of size. This finding is in agreement with the observation that catalyst performance was found to be stable over 300 h time on stream under WGSR conditions (see the Supporting Information).

Of particular interest for this work was investigating the effect of the KOH coating on the distribution and size of Pt nanoparticles on the alumina support before and after the WGSR in comparison to the uncoated catalyst. A catalyst sample coated with 7.5 wt% KOH was imaged before and after a similar WGSR [t_R (time-on-stream of WGSR) = 240 h]. An additional drying step at 150 °C for 4 h was added after coating the Pt/alumina catalyst with KOH.

Interestingly, a drastic change in nanoparticle size distribution was found for the KOH-coated catalyst (w = 7.5 wt%) before the WGSR. The mean Pt cluster diameter increased from 3.2 nm (for the uncoated catalyst) to 4.4 nm (center of Gaussian distribution) or 5.0 nm (arithmetic mean). Moreover, the size distribution was observed to be much broader with Pt particles up to 10 nm in size. Obviously, the mild salt impregnation pro-

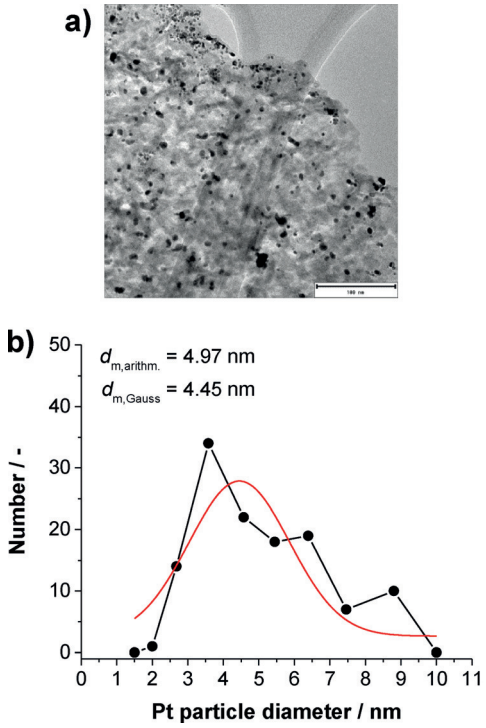

Figure 7. The KOH-coated Pt/alumina catalyst (w_{KOH} = 7.5 wt%, drying at T = 150 °C for 4 h) before the WGSR. a) Bright-field image acquired with a Philips CM300 transmission electron microscope at 300 kV; scale bar = 100 nm. b) Mean particle diameter obtained from evaluating 100 particles. Data are plotted in black, with Gaussian fit in red.

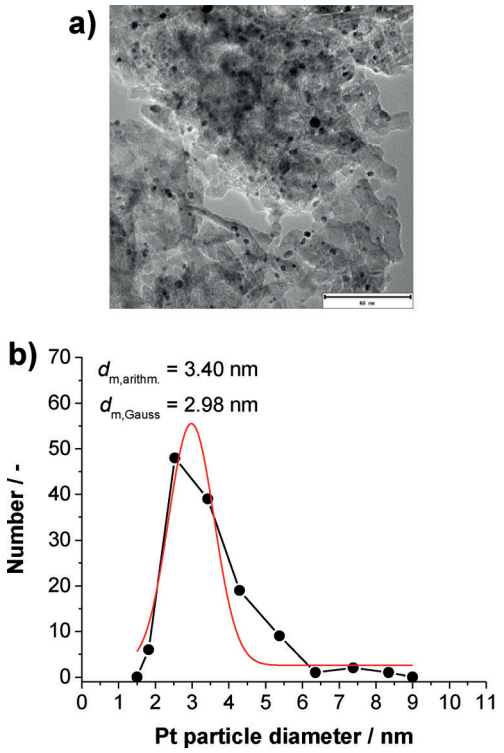

Figure 8. The KOH-coated Pt/alumina catalyst (w_{KOH} = 7.5 wt%, drying at T = 150 °C) after the WGSR (T = 200–230 °C, p_{CO} = 0.3–1.5 bar, p_{H_2O} = 0.25–1 bar, t_R = 240 h). a) Bright-field image acquired with a Philips CM300 transmission electron microscope at 300 kV; scale bar = 60 nm. b) Mean particle diameter obtained from evaluating 125 particles. Data are plotted in black, with Gaussian fit in red.

cess (including drying at T = 150 °C) already leads to a significant particle size redistribution.

We associated these observations with the formation of a basic aluminate layer on the support surface during salt impregnation and drying. Such a transformation of the support surface (alumina) to aluminate has been proved by our previous work on a similar system by using MAS NMR spectroscopy,[10] and reports on this phenomenon can also be found in the literature.[32] The Pt clusters presumably become more mobile on the basic aluminate support compared with alumina, which leads to some agglomeration of Pt nanoparticles.

Figure 8 shows the same catalyst as in Figure 7 but after its use in the WGSR.

The high-resolution TEM analysis after the reaction reveals another restructuring process of Pt nanoparticles during the WGSR. The mean Pt particle diameter of the catalyst is now 2.98 and 3.4 nm for the center of Gaussian distribution and arithmetic mean, respectively. The Pt nanoparticles are apparently redispersed on the alumina support during the WGSR. Consequently, the agglomeration process of Pt nanoparticles during the catalyst pretreatment and aluminate formation, seems to be at least partly reversible. In addition, the KOH-coated catalyst showed stability during 240 h time on stream in the WGSR, which indicated that the observed catalyst redistribution occurs quickly within the first few hours of the continuous experiment (see Figure 2). Following these studies using bright-field TEM, we also analyzed the catalyst samples by using scanning TEM (STEM) in combination with energy dispersive X-ray spectroscopy (EDS).

STEM with EDS

As the catalysts were found to undergo restructuring processes, we applied a second analytical technique to probe the location of potassium. High-angle annular dark-field (HAADF)-STEM measurements were performed in combination with EDS. The uncoated Pt/alumina catalyst was initially studied before its use in the WGSR (Figure 9).

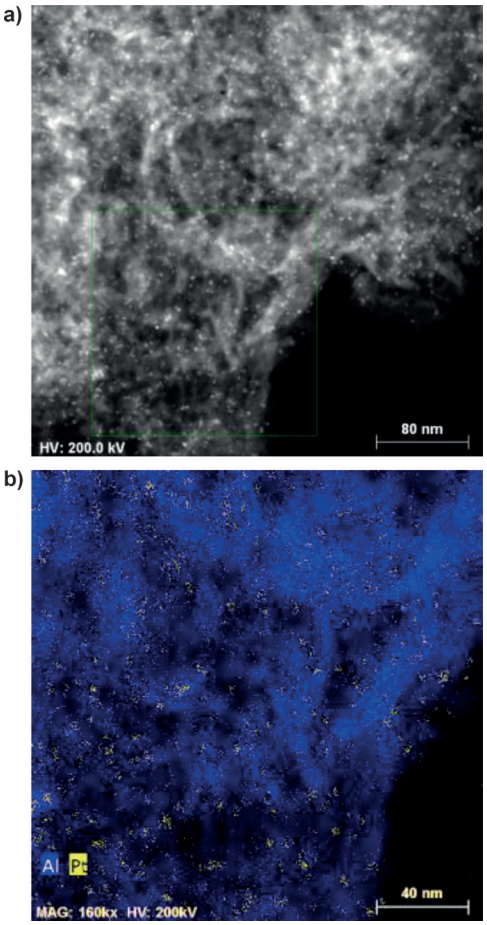

Figure 9. The uncoated Pt/alumina catalyst before the WGSR. a) HAADF-STEM image; scale bar = 80 nm; b) EDS map; scale bar = 40 nm. Both images were acquired with an FEI Titan 80–300 kV scanning transmission electron microscope at 200 kV by using an electron beam current of 0.6 nA and a Bruker SuperX X-ray detector.

The STEM image shows that the Pt nanoparticles are homogeneously distributed on the catalyst's alumina surface. In the EDS map, good agreement between the Pt signal (yellow) and the location in the HAADF-STEM image is found. An additional data set of a whole catalyst particle is provided in the Supporting Information. In the next step, we analyzed the same Pt/alumina catalyst after its use in the WGSR (T = 200–230 °C, p_{CO} = 0.3–1.5 bar, p_{H_2O} = 0.25–1 bar, t_R = 300 h; Figure 10).

The STEM–EDS analysis of the Pt/alumina catalyst after the WGSR reveals a homogeneous distribution of Pt particles. Their

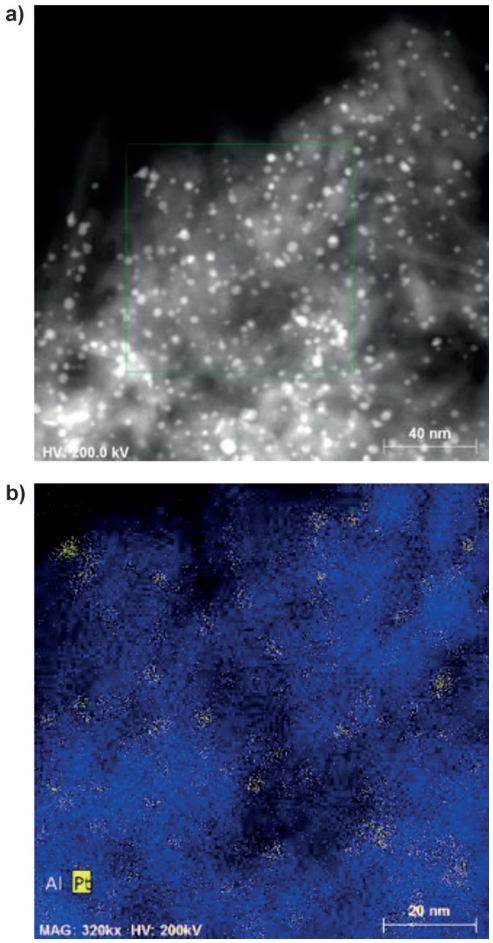

Figure 10. The uncoated Pt/alumina catalyst after the WGSR. a) HAADF-STEM image; scale bar = 40 nm; b) EDS map; scale bar = 20 nm. Both images were acquired with an FEI Titan 80–300 kV scanning transmission electron microscope at 200 kV by using an electron beam current of 0.6 nA and a Bruker SuperX X-ray detector.

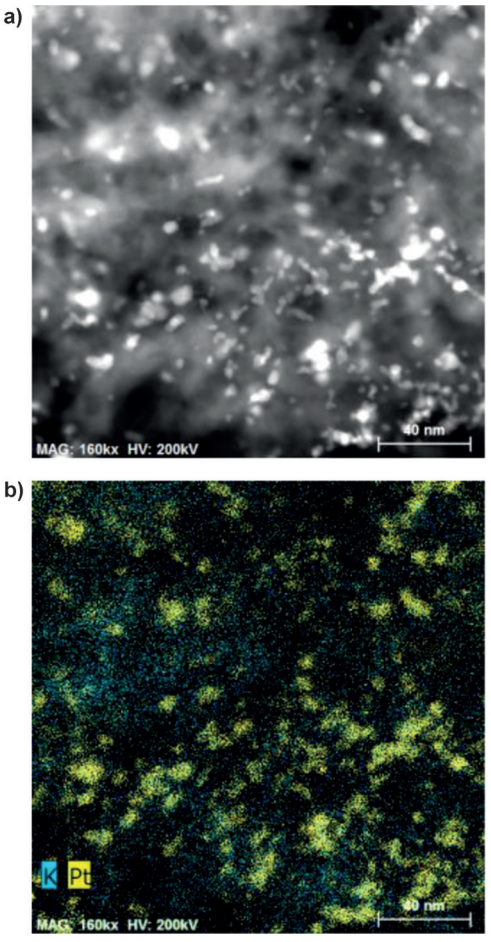

Figure 11. The KOH-coated Pt/alumina catalyst before the WGSR. a) HAADF-STEM image; scale bar = 40 nm; b) EDS map; scale bar = 40 nm. Both images were acquired with an FEI Titan 80–300 kV scanning transmission electron microscope at 200 kV by using an electron beam current of 0.6 nA and a Bruker SuperX X-ray detector.

particle sizes are similar to the results of the bright-field TEM analysis (d_{Pt} = 3–4 nm). The results are in good agreement with the experimental finding that the catalyst under observation has shown no sign of deactivation during 300 h time on stream in the WGSR (see the Supporting Information).

Of even higher interest is the investigation of the KOH-coated Pt/alumina catalyst (w_{KOH} = 7.5 wt%) before and after its use in the WGSR by applying the same HAADF-STEM–EDS technique. The images of the dried catalyst after impregnation with 7.5 wt% KOH are shown in Figure 11.

From the STEM image and the EDS map, a clustering of Pt nanoparticles with the formation of irregular structures is obvious, a finding that is in excellent agreement with the results of bright-field TEM analyses. The K atoms shown in turquoise appear to be homogeneously distributed over the alumina support before the catalyst use in the WGSR. These images showed that the KOH coating forms an aluminate layer on the alumina support material after the preparation process (drying at T = 150 °C).[10] No evidence for a specific Pt–K interaction is found.

In addition, a detailed, higher-resolution image of the same sample is shown in Figure 12.

By investigating the detailed image and EDS map of Pt nanoparticles impregnated with KOH, clustering behavior of Pt becomes evident. An individual Pt nanoparticle has a diameter less than 10 nm, but several particles tend to from larger agglomerates. Considering the distribution of KOH, we found a consistent spreading of K^+ on the alumina surface and in the proximity of Pt nanoparticles. The STEM–EDS images of the KOH-coated catalyst after its exposure to the WGSR are shown in Figures 13 and 14.

The analysis of the STEM images and EDS maps confirms the aforementioned Pt restructuring process (see the TEM section). Under WGSR conditions, Pt nanoparticles with a mean size of 5 nm form from the larger Pt agglomerates observed after the catalyst preparation. These observations are again in excellent agreement with the results of bright-field TEM experiments. A detailed, higher-resolution image of the same sample is shown in Figure 14. The maximum particle size (diameter) is 5 nm, but most of the particles have a smaller diameter (d_{Pt} = 3 nm). A

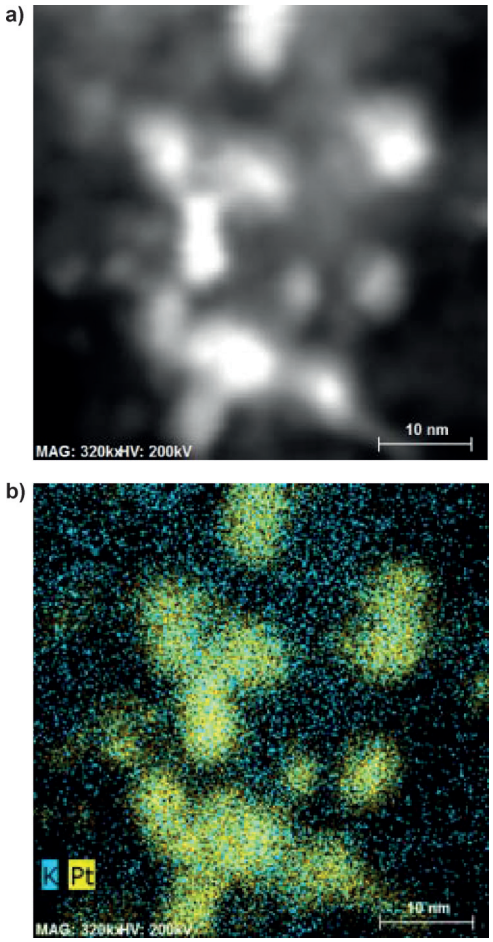

Figure 12. The KOH-coated Pt/alumina catalyst before the WGSR. a) Higher-resolution HAADF-STEM image; scale bar = 10 nm; b) higher-resolution EDS map; scale bar = 10 nm. Both images were acquired with an FEI Titan 80–300 kV scanning transmission electron microscope at 200 kV by using an electron beam current of 0.6 nA and a Bruker SuperX X-ray detector.

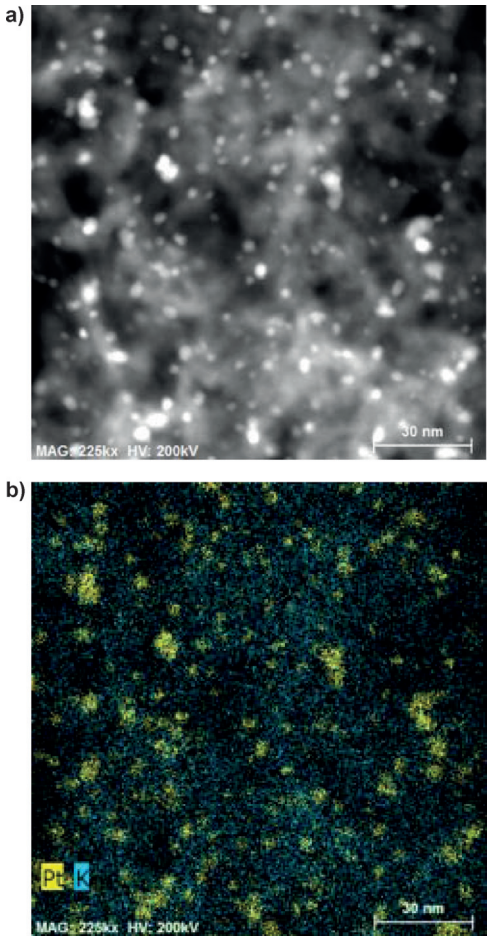

Figure 13. The KOH-coated Pt/alumina catalyst after the WGSR. a) HAADF-STEM image; scale bar = 30 nm; b) EDS map; scale bar = 30 nm. Both images were acquired with an FEI Titan 80–300 kV scanning transmission electron microscope at 200 kV by using an electron beam current of 0.6 nA and a Bruker SuperX X-ray detector.

dense distribution of K^+ on the alumina surface can be deduced from the EDS map.

The EDS map indicates that K^+ is homogeneously distributed both before and after the WGSR; it does not cluster as the Pt agglomerates, but remains uniform within the matrix. We suggest that in a K-containing matrix, it is highly likely that the Pt nanoparticles will come into contact with K atoms. Thus, HAADF-STEM investigations confirm that KOH doping of Pt nanoparticles results from salt impregnation without any calcination step during the catalyst preparation. We believe that the KOH loading of 7.5 wt% is sufficient to cause doping. The catalyst with a KOH loading of 7.5 wt% was found to have the highest catalytic activity. Higher KOH loadings would not improve the doping effect, but would lead to a higher degree of pore filling with negative effects on mass transfer.

Conclusions

We have demonstrated a convenient and effective method to significantly improve the performance of Pt/alumina catalysts for the water–gas shift reaction (WGSR) by coating the Pt/alumina catalyst with KOH at a loading of 7.5 wt%. At the same time, it has been confirmed that our earlier results describing activation of methanol steam reforming by potassium salt coatings[10] can be, at least in great part, understood by assuming a positive effect of the salt coating on the WGSR step of the methanol steam reforming reaction sequence. Our new approach is robust, highly reproducible, and very economical. There is no need to perform lengthy catalyst pretreatments such as calcination or preformation after the salt impregnation procedure.

By coating a commercial Pt/alumina catalyst with various loadings of alkali hydroxides, its activity for the WGSR increased six times, and KOH was found to be the most effective promoter. In the methanol steam reforming reaction,[10] the combination of alkali doping, basicity, and hygroscopicity is responsible for this remarkable effect. Because surface hydroxides play an important role in the catalytic cycle of the WGSR, the basic and hygroscopic nature of the hydroxide salts contributes to the improvement in catalyst performance. Contrary to our earlier experiments regarding the methanol steam reforming reaction, it seems that the WGSR is less sensitive to an

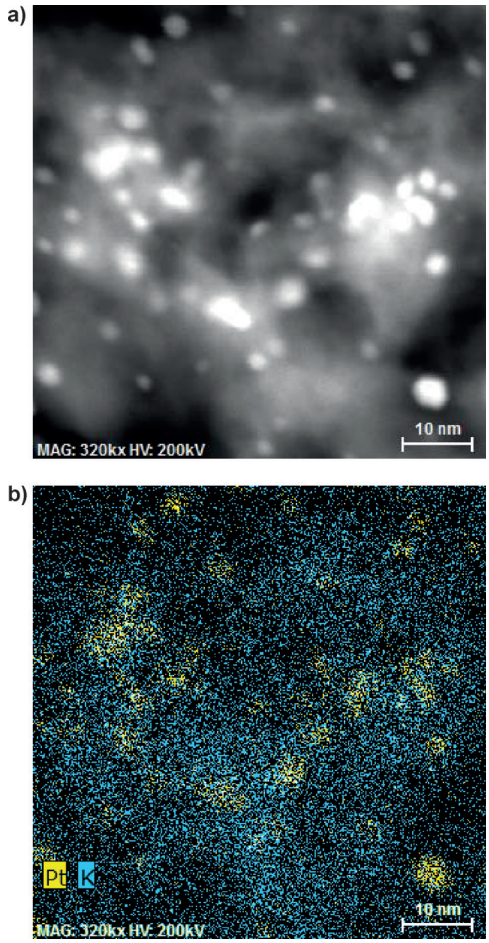

Figure 14. The KOH-coated Pt/alumina catalyst after the WGSR. a) Higher-resolution HAADF-STEM image; scale bar = 10 nm; b) higher-resolution EDS map; scale bar = 10 nm. Both images were acquired with an FEI Titan 80–300 kV scanning transmission electron microscope at 200 kV by using an electron beam current of 0.6 nA and a Bruker SuperX X-ray detector.

activity decline with high salt loadings. At least for LiOH, NaOH, and CsOH coatings, the 20 wt% salt loading was more active than the mass loading found to be optimum for KOH. In our kinetic studies, we showed that the reaction orders with respect to CO and H_2O partial pressures indicate only minor modification through KOH coating.

In a series of high-resolution TEM analyses, we demonstrated that the unmodified Pt/alumina catalyst is robust against the applied conditions of the WGSR. During the KOH coating process, the Pt/alumina catalyst undergoes an agglomeration process. Interestingly, this agglomeration is partly reversible under WGSR conditions, which leads to a highly active and stable system over 240 h time on stream. The active Pt nanoparticles tend to agglomerate during impregnation with KOH, but restructure under WGSR conditions. By using energy dispersive X-ray spectroscopy, the distribution of elements on the catalyst surface could be visualized, which confirmed all findings of bright-field TEM experiments. In addition, it was shown that for KOH loadings as low as 7.5 wt%, K^+ is homogeneously distributed on the alumina surface and is in close contact with the active Pt sites, which provides further evidence for a doping effect without a previous calcination step. To our knowledge, this is one of the first examples in which alkali doping of heterogeneous catalysts has been made visible by means of scanning TEM and energy dispersive X-ray spectroscopy techniques.

We suggest that the concept of modifying heterogeneous catalysts through molten salt coatings can be easily applied to other technically relevant reactions in the future. Moreover, this approach paves a way to a more rational and cost-effective catalyst optimization in heterogeneous catalysis.

Experimental Section

Materials

The Pt/alumina catalyst was purchased from Alfa Aesar (LOT: F02R004; precise Pt content = 4.86 wt%). LiOH (Merck, > 98%), NaOH (Merck, > 99%), KOH (Merck, > 85%, rest H_2O, K_2CO_3 < 1%), and CsOH (Fluka, 95%, rest H_2O) were used as stock solutions, and the amount of the hydroxide was determined by titration with HCl (1 M; Merck).

Synthesis of salt-modified catalysts

The calculated amount of Pt on the alumina support was immersed into a solution of the salt in high purity H_2O (typically V = 20 mL). After mixing for 30 min at T = 25 °C, the solvent was removed under vacuum (T = 60 °C, p = 50 mbar). The alkali hydroxide-coated catalyst samples were dried by heating up to 150 °C under vacuum (p < 0.1 mbar) for at least 4 h before WGSR experiments.

Catalytic experiments

The performance of the catalyst for the water–gasWGSR was evaluated in a continuously operated gas phase fixed-bed reactor (for details, see the Supporting Information). An equimolar mixture of CO and H_2O was evaporated and fed to the reactor. Typically, this mixture consisted of $p_{CO} = p_{H_2O}$ = 0.5 bar and 4 bar of the inert gas N_2 (e.g., V_{N_2} = 107.1 $mL_N min^{-1}$, V_{CO} = 13.3 $mL_N min^{-1}$, and V_{H_2O} = 13.3 $mL_N min^{-1}$). At the reactor outlet, unconverted H_2O was condensed and the product gas was analyzed by using GC (Varian CP 4900). Catalytic activities were given as TOFs, which was the total molar flow of CO_2 divided by the total molar amount of Pt in the reactor (typically $n_{Pt} = 1 \times 10^{-4}$ mol). The mass balance was closed by the quantification of the inert gas N_2, H_2, and remaining CO. During all experiments, no CH_4 was detected.

Kinetic experiments: Variation in partial pressure

Kinetic WGSR experiments were started under standard conditions (T = 230 °C, $p_{CO} = p_{H_2O}$ = 0.5 bar, p_{N_2} = 4 bar). Subsequently, temperature was varied from 200 to 230 °C (in steps of 10 °C). Afterward, p_{CO} was varied from 0.3 to 1.5 bar at a constant p_{H_2O} of 0.5 bar. τ was kept constant through variation of the flow in N_2. The variation in p_{CO} was finished by returning to standard conditions. For one step of variation in p_{CO}, at least 12 h were spent. p_{H_2O} was varied from 0.25 to 1.0 bar, whereas p_{CO} was kept constant at 0.5 bar. Finally, standard conditions were reestablished to ensure a stable performance or no deactivation. For one step of variation in p_{H_2O}, at least 8 h were spent. The results were evaluated by

using the power law model as described in the Results and Discussion section.

TEM experiments

Catalyst samples were analyzed with a Philips CM300 transmission electron microscope operating at 300 kV voltage in the bright-field mode and equipped with an LaB_6 gun. Catalyst samples were dispersed in cyclohexane and impregnated onto Cu lacey carbon TEM grids (Plato). Images were taken with a charge-coupled device camera (2048×2048 pixels, Tietz TVIPS, particle size analysis in ImageJ, at least 100 particles counted for Pt particle size distribution). Data were fit with a standard Gaussian function in Origin 9.1 G.

HAADF-STEM–EDS experiments

The HAADF-STEM analysis was performed with an FEI Titan 80–300 kV scanning transmission electron microscope equipped with a SuperTwin objective lens with Cs = 1.2 mm at the National Center for Electron Microscopy, Molecular Foundry, Lawrence Berkeley National Lab. The EDS spectra were acquired with four windowless silicon drift detectors with a total solid angle of 0.7 sr. The catalyst samples were impregnated onto Cu lacey carbon TEM grids (Ted Pella) and analyzed at 200 kV (Schottky field emission gun). Imaging conditions resulted in a convergence semiangle of 10 mrad and an HAADF detector inner semiangle of 50 mrad. The electron beam current was in the range of 300–600 nA, with a maximum acquisition time of 600 s. The image size was 1024×1024. For EDX mapping, an area of 512×512 pixels was selected. All data were processed with Gatan's Digital Micrograph/Image J software (for images) or Bruker's ESPRIT software (for EDS data evaluation).

Acknowledgements

We acknowledge financial support by the EU through its ERC Advanced Investigator Grant (grant no. 267376, to P.W.) We also acknowledge Deutsche Forschungsgemeinschaft (DFG) for supporting some of the analytic work through its Excellence Cluster "Engineering of Advanced Materials" in the framework of the excellence initiative. Furthermore, we thank the Center for Nanoanalysis and Electron Microscopy (CENEM), Erlangen for assistance with the TEM measurements. We acknowledge support of the National Center for Electron Microscopy, Molecular Foundry, Lawrence Berkeley Lab, which is supported by the U.S. Department of Energy (contract no. DE-AC02-05CH11231).

Keywords: electron microscopy · heterogeneous catalysis · ionic liquids · platinum · water–gas shift reaction

[1] a) C. Ratnasamy, J. P. Wagner, *Catal. Rev.* **2009**, *51*, 325–440; b) D. S. Newsome, *Catal. Rev.* **1980**, *21*, 275–318.
[2] a) S. Werner, N. Szesni, M. Kaiser, R. W. Fischer, M. Haumann, P. Wasserscheid, *ChemCatChem* **2010**, *2*, 1399–1402; b) J. R. Ladebeck, J. P. Wagner in *Handbook of fuel cells*, John Wiley & Sons, New York, **2010**.
[3] R. Farrauto, S. Hwang, L. Shore, W. Ruettinger, J. Lampert, T. Giroux, Y. Liu, O. Llinich, *Annu. Rev. Mater. Res.* **2003**, *33*, 1–27.
[4] R. Kam, J. Scott, R. Amal, C. Selomulya, *Chem. Eng. Sci.* **2010**, *65*, 6461–6470.
[5] J. A. Rodriguez, J. C. Hanson, D. Stacchiola, S. D. Senanayake, *Phys. Chem. Chem. Phys.* **2013**, *15*, 12004–12025.
[6] D. C. Grenoble, M. M. Estadt, *J. Catal.* **1981**, *67*, 90–102.
[7] P. Panagiotopoulou, D. I. Kondarides, *Catal. Today* **2006**, *112*, 49–52.
[8] Y. Zhai, D. Pierre, R. Si, W. Deng, P. Ferrin, A. U. Nilekar, G. Peng, J. A. Herron, D. C. Bell, H. Saltsbrug, M. Mavrikakis, M. Flytzani-Stephanopoulos, *Science* **2010**, *329*, 1633–1636.
[9] M. Kusche, F. Enzenberger, S. Bajus, H. Niedermeyer, A. Bösmann, A. Kaftan, M. Laurin, J. Libuda, P. Wasserscheid, *Angew. Chem. Int. Ed.* **2013**, *52*, 5028–5032; *Angew. Chem.* **2013**, *125*, 5132–5136.
[10] M. Kusche, F. Agel, N. N. Bhriain, A. Kaftan, M. Laurin, J. Libuda, P. Wasserscheid, *ChemSusChem* **2014**, *7*, 2516–2526.
[11] D. R. Palo, R. A. Dagle, J. D. Holladay, *Chem. Rev.* **2007**, *107*, 3992–4021.
[12] U. Kernchen, B. Etzold, W. Korth, A. Jess, *Chem. Eng. Technol.* **2007**, *30*, 985–994.
[13] V. A. Cocalia, A. E: Visser, R. D. Rogers, J. D. Holbrey in *Ionic Liquids in Synthesis* (Eds.: P. Wasserscheid, T. Welton), Wiley-VCH, Weinheim, **2008**, pp. 89–102.
[14] a) T. Herrmann, L. Rößmann, M. Lucas, P. Claus, *Chem. Commun.* **2011**, *47*, 12310–12312; b) N. Wörz, J. Arras, P. Claus, *Appl. Catal. A* **2011**, *391*, 319–324.
[15] a) M. Sobota, M. Happel, M. Amende, N. Paape, P. Wasserscheid, M. Laurin, J. Libuda, *Adv. Mater.* **2011**, *23*, 2617–2621; b) H.-P. Steinrück, J. Libuda, P. Wasserscheid, T. Cremer, C. Kolbeck, M. Laurin, F. Maier, M. Sobota, P. S. Schulz, M. Stark, *Adv. Mater.* **2011**, *23*, 2571–2587.
[16] N. Taccardi, D. Assenbaum, M. E. M. Berger, A. Bösmann, F. Enzenberger, R. Wölfel, S. Neuendorf, V. Göcke, N. Schödel, H.-J. Maass, H. Kistenmacher, P. Wasserscheid, *Green Chem.* **2010**, *12*, 1150–1156.
[17] G. G. Diogenov, G. S. Sergeeva, *Zh. Neorg. Khim.* **1965**, *10*, 292–294.
[18] M. Kisinkova, G. Pirug, H. P. Bonzel, *Surf. Sci.* **1983**, *133*, 321–343.
[19] H. P. Bonzel, *Surf. Sci. Rep.* **1988**, *81*, 43–125.
[20] S. Derrouiche, P. Gravejat, B. Bassou, D. Bianchi, *Appl. Surf. Sci.* **2007**, *253*, 5894–5898.
[21] B. Zugic, S. Zhang, D. C. Bell, F. F. Tao, M. Flytzani-Stephanopoulos, *J. Am. Chem. Soc.* **2014**, *136*, 3238–3245.
[22] H. N. Evin, G. Jacobs, J. Ruiz-Martinez, U. M. Graham, A. Dozier, G. Thomas, B. H. Davis, *Catal. Lett.* **2008**, *122*, 9–19.
[23] B. Liu, T. Huang, Z. Zhang, Z. Wang, Y. Zhang, J. Li, *Catal. Sci. Technol.* **2014**, *4*, 1286–1292.
[24] G. Jacobs, B. H. Davis, *Int. J. Hydrogen Energy* **2010**, *35*, 3522–3536.
[25] C. M. Kalamaras, G. G. Olympiou, A. M. Efstathiou, *Catal. Today* **2008**, *138*, 228–234.
[26] D. W. Flaherty, W.-Y. Yu, Z. D. Pozun, G. Henkelman, C. B. Mullins, *J. Catal.* **2011**, *282*, 278–288.
[27] F. C. Meunier, *Catal. Today* **2010**, *155*, 164–171.
[28] L. C. Grabow, A. A. Gokhale, S. T. Evans, J. A. Dumesic, M. Mavrikakis, *J. Phys. Chem. C* **2008**, *112*, 4608–4617.
[29] C. M. Kalamaras, I. D. Gonzales, R. M. Navarro, J. L. G. Fierro, A. M. Efstathiou, *J. Phys. Chem. C* **2011**, *115*, 11595–11610.
[30] a) R. J. Smith, M. Loganathan, M. S. Shantha, *Int. J. Chem. React. Eng.* **2010**, *8*, 1–28; b) A. A. Phatak, N. Koryabkina, S. Rai, J. L. Ratts, W. Ruettinger, R. J. Farrauto, G. E. Blau, W. N. Delgass, F. H. Ribeiro, *Catal. Today* **2007**, *123*, 224–234.
[31] G. G. Olympiou, C. M. Kalamaras, C. D. Zeinalipour-Yazdi, A. M. Efstathiou, *Catal. Today* **2007**, *127*, 304–318.
[32] D. Müller, W. Gessner, A. Samoson, E. Lippmaa, G. Scheler, *J. Chem. Soc. Dalton Trans.* **1986**, 1277–1281.

Received: October 10, 2014
Published online on January 29, 2015

